

# Bending, Buckling and Vibrations Analysis of the Graphene Nanoplate Using the Modified Couple Stress Theory

Majid ESKANDARI SHAHRAKI\*, Mahmoud SHARIATI\*\*, Naser ASIABAN\*\*\*, Jafar ESKANDARI JAM\*\*\*\*

\*Aerospace Engineering, Ferdowsi University of Mashhad, Mashhad, Iran, E-mail: mjdeskandari@gmail.com

\*\*Mechanical Engineering, Ferdowsi University of Mashhad, Mashhad, Iran, E-mail: mshariati44@gmail.com

\*\*\*Mechanical Engineering, Ferdowsi University of Mashhad, Mashhad, Iran, E-mail: naser.asiaban@mail.um.ac.ir

\*\*\*\*Mechanical Engineering, Malek-Ashtar University of Technology, Tehran, Iran, E-mail: jejam@mail.com

crossref <http://dx.doi.org/10.5755/j02.mech.25299>

## 1. Introduction

The atomic and molecular scale test is known as the safest method for the study of materials in small-scales. In this method, the nanostructures are studied in real dimensions. The atomic force microscopy (AFM) is used to apply different mechanical loads on nanoplates and measure their responses against those load in order to determine the mechanical properties of the nanoplate. The difficulty of controlling the test conditions at this scale, high economic costs and time-consuming processes are some setbacks of this method. Therefore, it is used only to validate other simple and low-cost methods.

Atomic simulation is another solution for studying small-scale structures. In this method, the behavior of atoms and molecules is examined by considering the intermolecular and interatomic effects on their motions, which eventually involves the total deformation of the body. In the case of large deformations and multi atomic scale the computational costs is too high, so this method is only used for small deformation problems.

Given the limitations of the aforementioned methods for studying nanostructures, researchers have been looking for simpler solutions for nanostructures. Modeling small-scale structures using continuum mechanics is another solution to this problem. There are a variety of size-dependent continuum theories that consider size effects, some of these theories are; micromorphic theory, microstructural theory, micropolar theory, Kurt's theory, non-local theory, modified couple stress theory and strain gradient elasticity. All of which are the developed notion of classical field theories, which include size effects.

## 2. Modified couple stress theory

In 2002 Yang et al. [1] proposed a modified couple stress model by modifying the theory proposed by Toppin [2], Mindlin and Thursten [3], Quitter [4] and Mindlin [5] in 1964. The modified couple stress theory consists of one material length scale parameter for projection of the size effect, whereas the classical couple stress theory has two material length scale parameters. In the modified couple stress theory, the strain energy density in the three-dimensional vertical coordinates for a body bounded by the volume  $V$  and the area  $\Omega$  [6], is expressed as the follows:

$$U = \frac{1}{2} \int_V (\sigma_{ij} \varepsilon_{ij} + m_{ij} \chi_{ij}) dV \quad i, j = 1, 2, 3, \quad (1)$$

where:

$$\varepsilon_{ij} = \frac{1}{2} (u_{i,j} + u_{j,i}), \quad (2)$$

$$\chi_{ij} = \frac{1}{2} (\theta_{i,j} + \theta_{j,i}), \quad (3)$$

$\chi_{ij}$  and  $\varepsilon_{ij}$  are the symmetric parts of the curvature and strain tensors;  $\theta_i$  and  $u_i$  are the displacement and the rotational vectors, respectively.

$$\theta_i = \frac{1}{2} e_{ijk} u_{k,j}, \quad (4)$$

$\sigma_{ij}$ , the stress tensor, and  $m_{i,j}$ , the deviatoric part of the couple stress tensor, are defined as:

$$\sigma_{ij} = \lambda \varepsilon_{kk} \delta_{ij} + 2\mu \varepsilon_{ij}, \quad (5)$$

$$m_{i,j} = 2\mu l^2 \chi_{ij}, \quad (6)$$

where:  $\lambda$  and  $\mu$  are the lame constants;  $\delta_{ij}$  is the Kronecker delta and  $l$  is the material length scale parameter. From Eqs. (3) and (6) it can be seen that  $\chi_{ij}$  and  $m_{ij}$  are symmetric.

## 3. Mindlin's plate model

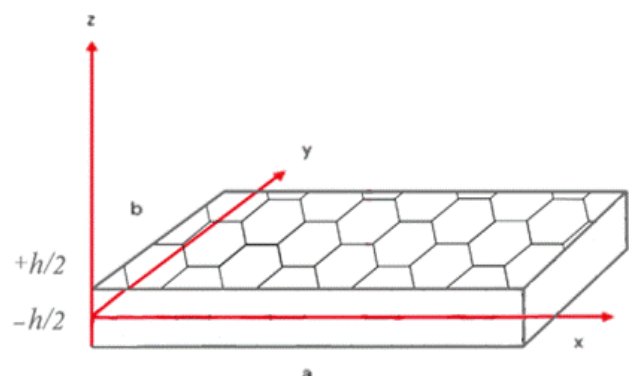


Fig. 1 A schematic of the nanoplate and axes

The displacement equations for the Mindlin's plate are defined as [8]:

$$\begin{aligned} u_1(x, y, z, t) &= u(x, y, t) + z\varphi_x \\ u_2(x, y, z, t) &= v(x, y, t) + z\varphi_y, \\ u_3(x, y, z, t) &= w(x, y, t), \end{aligned} \quad (7)$$

where:  $\varphi_x$  and  $\varphi_y$  are the rotations of the normal vector around the  $x$  and  $y$  axis respectively, and  $w$  is the midpoint displacement of the plate in the  $z$ -direction. The strain and stress tensors, the symmetric part of the curvature tensor, and the rotational vector for the Mindlin's plate is obtained as follows:

$$\varepsilon_{xx} = z \frac{\partial \varphi_x}{\partial x}, \quad (8)$$

$$\varepsilon_{yy} = z \frac{\partial \varphi_y}{\partial y}, \quad (9)$$

$$\varepsilon_{zz} = 0, \quad (10)$$

$$\varepsilon_{xy} = \varepsilon_{yx} = \frac{1}{2} z \left( \frac{\partial \varphi_x}{\partial y} + \frac{\partial \varphi_y}{\partial x} \right), \quad (11)$$

$$\varepsilon_{xz} = \varepsilon_{zx} = \frac{1}{2} \left( \frac{\partial w}{\partial x} + \varphi_x \right), \quad (12)$$

$$\varepsilon_{yz} = \varepsilon_{zy} = \frac{1}{2} \left( \frac{\partial w}{\partial y} + \varphi_y \right), \quad (13)$$

$$\theta_x = \frac{1}{2} \left( \frac{\partial w}{\partial y} - \varphi_y \right), \quad (14)$$

$$\theta_y = \frac{1}{2} \left( \varphi_x - \frac{\partial w}{\partial x} \right), \quad (15)$$

$$\theta_z = \frac{1}{2} z \left( \frac{\partial^2 w}{\partial x \partial y} - \frac{\partial \varphi_x}{\partial y} \right), \quad (16)$$

$$x_{xx} = \frac{1}{2} \left( \frac{\partial^2 w}{\partial x \partial y} - \frac{\partial \varphi_y}{\partial x} \right), \quad (17)$$

$$x_{yy} = \frac{1}{2} \left( \frac{\partial \varphi_x}{\partial y} - \frac{\partial^2 w}{\partial x \partial y} \right), \quad (18)$$

$$x_{zz} = \frac{1}{2} \left( \frac{\partial \varphi_y}{\partial x} - \frac{\partial \varphi_x}{\partial y} \right), \quad (19)$$

$$x_{xy} = \frac{1}{4} \left( \frac{\partial^2 w}{\partial y^2} - \frac{\partial^2 w}{\partial x^2} + \frac{\partial \varphi_y}{\partial x} - \frac{\partial \varphi_x}{\partial y} \right), \quad (20)$$

$$x_{xz} = \frac{1}{4} z \left( \frac{\partial^2 \varphi_y}{\partial x^2} - \frac{\partial^2 \varphi_x}{\partial y \partial x} \right), \quad (21)$$

$$x_{yz} = \frac{1}{4} z \left( \frac{\partial^2 \varphi_y}{\partial x \partial y} - \frac{\partial^2 \varphi_x}{\partial y^2} \right), \quad (22)$$

$$\sigma_{xx} = (\lambda + 2\mu) z \frac{\partial \varphi_y}{\partial x} + \lambda z \frac{\partial \varphi_y}{\partial y}, \quad (23)$$

$$\sigma_{yy} = \lambda z \frac{\partial \varphi_x}{\partial x} + (\lambda + 2\mu) z \frac{\partial \varphi_y}{\partial y}, \quad (24)$$

$$\sigma_{zz} = \lambda \left( z \frac{\partial \varphi_x}{\partial x} + z \frac{\partial \varphi_y}{\partial y} \right), \quad (25)$$

$$\sigma_{yx} = \sigma_{xy} = \mu z \left( \frac{\partial \varphi_x}{\partial y} + z \frac{\partial \varphi_y}{\partial x} \right), \quad (26)$$

$$\sigma_{xz} = \sigma_{zx} = \mu \left( \frac{\partial w}{\partial x} + \varphi_x \right), \quad (27)$$

$$\sigma_{yz} = \sigma_{zy} = \mu \left( \frac{\partial w}{\partial y} + \varphi_y \right). \quad (28)$$

The variation of the strain energy is expressed as follows:

$$\begin{aligned} \delta U = \int_V (\sigma_{xx} \delta \varepsilon_{xx} + \sigma_{yy} \delta \varepsilon_{yy} + 2\sigma_{xy} \delta \varepsilon_{xy} + \\ + 2\sigma_{xz} \delta \varepsilon_{xz} + 2\sigma_{yz} \delta \varepsilon_{yz} + m_{xx} \delta x_{xx} + m_{yy} \delta x_{yy} + \\ + m_{zz} \delta x_{zz} + 2m_{xy} \delta x_{xy} + 2m_{xz} \delta x_{xz} + 2m_{yz} \delta x_{yz}) dV. \end{aligned} \quad (29)$$

For the sake of simplification, the coefficient of each variable in the above equation is named from  $F_1$  to  $F_{15}$  and this equation can be rewritten as shown below:

$$\begin{aligned} \delta U = \int_V (F_1 \delta w_{,xx} + F_2 \delta w_{,yy} + F_3 \delta w_{,xy} + F_4 \delta w_{,x} \\ + F_5 \delta w_{,y} + F_6 \delta \varphi_{x,yy} + F_7 \delta \varphi_{y,xx} + F_8 \delta \varphi_{y,xy} + \\ + F_9 \delta \varphi_{x,xy} + F_{10} \delta \varphi_{x,x} + F_{11} \delta \varphi_{y,y} + F_{12} \delta \varphi_{x,y} + \\ + F_{13} \delta \varphi_{y,x} + F_{14} \delta \varphi_x + F_{15} \delta \varphi_y) dV. \end{aligned} \quad (30)$$

where:

$$F_1 = -\frac{1}{4} \mu l^2 \left( \frac{\partial^2 w}{\partial y^2} - \frac{\partial^2 w}{\partial x^2} + \frac{\partial \varphi_x}{\partial x} - \frac{\partial \varphi_y}{\partial y} \right), \quad (31)$$

$$F_2 = \frac{1}{4} \mu l^2 \left( \frac{\partial^2 w}{\partial y^2} - \frac{\partial^2 w}{\partial x^2} + \frac{\partial \varphi_x}{\partial x} - \frac{\partial \varphi_y}{\partial y} \right), \quad (32)$$

$$F_3 = \mu l^2 \left( \frac{\partial^2 w}{\partial x \partial y} - \frac{1}{2} \frac{\partial \varphi_y}{\partial x} - \frac{1}{2} \frac{\partial \varphi_x}{\partial y} \right), \quad (33)$$

$$F_4 = \mu \left( \frac{\partial w}{\partial x} + \varphi_x \right), \quad (34)$$

$$F_5 = \mu \left( \frac{\partial w}{\partial y} + \varphi_y \right), \quad (35)$$

$$F_6 = F_8 = \frac{1}{4} \mu l^2 z^2 \left( \frac{\partial^2 \varphi_y}{\partial x \partial y} - \frac{\partial^2 \varphi_x}{\partial y^2} \right), \quad (36)$$

$$F_7 = F_9 = \frac{1}{4} \mu l^2 z^2 \left( \frac{\partial^2 \varphi_y}{\partial x^2} - \frac{\partial^2 \varphi_x}{\partial x \partial y} \right), \quad (37)$$

$$F_{10} = (\lambda + 2\mu) z^2 \frac{\partial \varphi_x}{\partial x} + \lambda z^2 \frac{\partial \varphi_y}{\partial y} + \frac{1}{4} \mu l^2 \left( \frac{\partial^2 w}{\partial y^2} - \frac{\partial^2 w}{\partial x^2} + \frac{\partial \varphi_x}{\partial x} - \frac{\partial \varphi_y}{\partial y} \right), \quad (38)$$

$$F_{11} = \lambda z^2 \frac{\partial \varphi_x}{\partial x} + (\lambda + 2\mu) z^2 \frac{\partial \varphi_y}{\partial y} - \frac{1}{4} \mu l^2 \left( \frac{\partial^2 w}{\partial y^2} - \frac{\partial^2 w}{\partial x^2} + \frac{\partial \varphi_x}{\partial x} - \frac{\partial \varphi_y}{\partial y} \right), \quad (39)$$

$$F_{12} = \mu z^2 \left( \frac{\partial \varphi_x}{\partial y} + \frac{\partial \varphi_y}{\partial x} \right) + \mu l^2 \left( \frac{\partial \varphi_x}{\partial y} + \frac{1}{2} \frac{\partial \varphi_y}{\partial x} - \frac{1}{2} \frac{\partial^2 w}{\partial x \partial y} \right), \quad (40)$$

$$F_{13} = \mu z^2 \left( \frac{\partial \varphi_x}{\partial y} + \frac{\partial \varphi_y}{\partial x} \right) + \mu l^2 \left( \frac{\partial \varphi_y}{\partial x} - \frac{1}{2} \frac{\partial^2 w}{\partial x \partial y} - \frac{1}{2} \frac{\partial^2 \varphi_x}{\partial y} \right), \quad (41)$$

$$F_{14} = \mu \left( \frac{\partial w}{\partial x} + \varphi_x \right), \quad (42)$$

$$F_{15} = \mu \left( \frac{\partial w}{\partial y} + \varphi_y \right). \quad (43)$$

#### 4. The buckling force

For a rectangular plate with length  $a$ , width  $b$  and thickness  $h$ , under the axial forces  $(P_{xy}, P_y, P_x)$ , the buckling force is obtained as shown in equation (44) [7]:

$$P_x \frac{\partial^2 w}{\partial x^2} + 2P_{xy} \frac{\partial^2 w}{\partial x \partial y} + P_y \frac{\partial^2 w}{\partial y^2} = q(x, y), \quad (44)$$

where:  $P_x$  is the Axial force along the  $x$  axis;  $P_y$  is the Axial force along the  $y$  axis;  $P_{xy}$  is the shear force in the  $xy$  plane, and  $q(x, y)$  is the out-of-plane force.

#### 5. Virtual work of the external forces

In these kind of problems, the virtual work of three kinds of external forces are included in the solutions, if the

middle-plane and the middle-perimeter of the plate are shown as  $\Omega$  and  $\Gamma$  respectively, these virtual works are [8]:

1. The virtual work done by the body forces, which is applied on the volum  $V = \Omega \times (-h/2, h/2)$ .
2. The virtual work done by the surface tractions at the upper and lower surfaces  $\Omega$ .
3. The virtual work done by the shear tractions on the lateral surfaces,  $S = \Gamma \times (-h/2, h/2)$ .

If  $(f_x, f_y, f_z)$  are the body forces,  $(c_x, c_y, c_z)$  are the body couples,  $(q_x, q_y, q_z)$  are the forces acting on the  $\Omega$  plane,  $(t_x, t_y, t_z)$  are the Cauchy's tractions and  $(S_x, S_y, S_z)$  are surface couples the Variations of the virtual work is expressed as:

$$\delta w = -[\int_{\Omega} (f_x \delta u + f_y \delta v + f_z \delta w + q_x \delta u + q_y \delta v + q_z \delta w + c_x \delta \theta_x + c_y \delta \theta_y + c_z \delta \theta_z) dx dy + \int_{\Gamma} (t_x \delta u + t_y \delta v + t_z \delta w + s_x \delta \theta_x + s_y \delta \theta_y + s_z \delta \theta_z)]. \quad (45)$$

Given that in this study only the external force  $q_z$  was applied, virtual work becomes:

$$\delta w = \int_0^a \int_0^b q(x, y) \delta w(x, y) dx dy, \quad (46)$$

the variation of kinetic energy is obtained as:

$$\delta T = \int_A \int_{-\frac{h}{2}}^{\frac{h}{2}} \rho (\dot{u}_1 \delta \dot{u}_1 + \dot{u}_2 \delta \dot{u}_2 + \dot{u}_3 \delta \dot{u}_3) dA dz = \int_A \left[ \rho h \dot{w} \delta \dot{w} + \frac{\rho h^3}{12} (\dot{\varphi}_x \delta \dot{\varphi}_x + \dot{\varphi}_y \delta \dot{\varphi}_y) \right] dA, \quad (47)$$

where:  $\rho$  is the density.

Finally using the Hamilton's principle, it can be said that [9]:

$$\int_0^T (\delta T - (\delta U - \delta w)) dt = 0, \quad (48)$$

where:  $T$  is the kinetic energy;  $U$  is the strain energy, and  $w$  is the work of the external forces.

#### 6. The final governing equations of the plate after applying the buckling and external forces

Using Hamilton's principle, Eq. (48), and the Eqs. from (44) to (47), the governing equations of the plate including the buckling and external forces are obtained as follows:

$$\left[ \int_{-h/2}^{h/2} \left( \frac{\partial^2 F_1}{\partial x^2} - \frac{\partial F_4}{\partial x} + \frac{\partial^2 F_2}{\partial y^2} + \frac{\partial^2 F_3}{\partial x \partial y} - \frac{\partial F_5}{\partial y} \right) dz \right] = q(x, y) + \rho h \frac{\partial^2 w}{\partial t^2}, \quad (49)$$

$$\int_{-h/2}^{h/2} \left( \frac{\partial^2 F_6}{\partial y^2} + \frac{\partial^2 F_9}{\partial x \partial y} - \frac{\partial F_{12}}{\partial y} - \frac{\partial F_{10}}{\partial x} + F_{14} \right) dz = \frac{\rho h^3}{12} \frac{\partial^2 \varphi_x}{\partial t^2}, \quad (50)$$

$$\int_{-h/2}^{h/2} \left( \frac{\partial^2 F_7}{\partial x^2} - \frac{\partial F_{13}}{\partial x} + \frac{\partial^2 F_8}{\partial x \partial y} - \frac{\partial F_{11}}{\partial y} + F_{15} \right) dz = \frac{\rho h^3}{12} \frac{\partial^2 \varphi_y}{\partial t^2}. \quad (51)$$

### 7. Obtaining the general governing equation of the Mindlin's plate (including buckling, bending and vibrations)

Considering the following constants:

$$C_1 = \frac{1}{4} \mu l^2 h, \quad (52)$$

$$C_2 = \mu h k_s, \quad (53)$$

$$C_3 = \frac{1}{4} \mu l^2 I^2, \quad (54)$$

$$C_4 = -\mu I_2 - \mu l^2 h, \quad (55)$$

$$C_5 = -\lambda I_2 - 2\mu I_2 - \frac{1}{4} \mu l^2 h, \quad (56)$$

$$C_6 = -\mu I_2 - \lambda I_2 + \frac{3}{4} \mu l^2 h, \quad (57)$$

$$C_7 = \rho h, \quad (58)$$

$$C_8 = \frac{\rho h^3}{12}, \quad (59)$$

$$k_s = \frac{5}{6} = 0.8 \quad (60)$$

where:

$$I_i = \int_{-h/2}^{h/2} Z^i dz \quad (61)$$

the general governing equation of the Mindlin's plate will become:

$$\begin{aligned} & 2C_1 \frac{\partial^2 w}{\partial x^2 \partial y^2} + C_1 \frac{\partial^2 w}{\partial x^4} + C_1 \frac{\partial^2 w}{\partial y^4} - C_2 \frac{\partial^2 w}{\partial x^2} - \\ & - C_2 \frac{\partial^2 w}{\partial y^2} - C_1 \frac{\partial^3 \varphi_x}{\partial x^3} - C_1 \frac{\partial^3 \varphi_y}{\partial y^3} - C_1 \frac{\partial^3 \varphi_y}{\partial x^2 \partial y} - \\ & - C_2 \frac{\partial \varphi_x}{\partial x} - C_2 \frac{\partial \varphi_y}{\partial y} = q(x, y) + C_7 \frac{\partial^2 w}{\partial t^2}, \end{aligned} \quad (62)$$

$$\begin{aligned} & C_3 \left( \frac{\partial^4 \varphi_y}{\partial x \partial y^3} + \frac{\partial^4 \varphi_x}{\partial y^4} + \frac{\partial^4 \varphi_y}{\partial x^3 \partial y} - \frac{\partial^4 \varphi_x}{\partial x^2 \partial y^2} \right) + C_4 \frac{\partial^2 \varphi_x}{\partial y^2} \\ & + C_5 \frac{\partial^2 \varphi_x}{\partial x^2} + C_6 \frac{\partial^2 \varphi_y}{\partial x \partial y} + C_1 \frac{\partial^2 w}{\partial x \partial y^2} + \\ & + C_1 \frac{\partial^2 w}{\partial x^3} + C_2 \frac{\partial w}{\partial x} + C_2 \varphi_x = C_8 \frac{\partial^2 \varphi_x}{\partial t^2}, \end{aligned} \quad (63)$$

$$\begin{aligned} & C_3 \left( \frac{\partial^2 \varphi_y}{\partial x^4} - \frac{\partial^4 \varphi_x}{\partial x \partial y} + \frac{\partial^4 \varphi_y}{\partial x^2 \partial y^2} - \frac{\partial^4 \varphi_x}{\partial x \partial y^3} \right) + C_6 \frac{\partial^2 \varphi_x}{\partial x \partial y} \\ & + C_4 \frac{\partial^2 \varphi_y}{\partial x^2} + C_5 \frac{\partial^2 \varphi_y}{\partial y^2} + C_1 \frac{\partial^3 w}{\partial y \partial x^2} + \\ & + C_1 \frac{\partial^3 w}{\partial y^3} + C_2 \frac{\partial w}{\partial y} + C_2 \varphi_x = C_8 \frac{\partial^2 \varphi_y}{\partial t^2}. \end{aligned} \quad (64)$$

### 8. Solution of the governing equations using Navier's method

The Navier's solution is applicable to the rectangular plates which have simply supported boundary conditions on all edges. Since the boundary conditions are spontaneously satisfied in this method, the unknown functions of the plate's mid-plane were assumed to be double trigonometric series [8]:

$$W(x, y, t) = \sum_{m=1}^{\infty} \sum_{n=1}^{\infty} W_{mn} \sin \alpha x \sin \beta y e^{i\omega t}, \quad (65)$$

$$\varphi_x(x, y, t) = \sum_{m=1}^{\infty} \sum_{n=1}^{\infty} X_{mn} \cos \alpha x \sin \beta y e^{i\omega t}, \quad (66)$$

$$\varphi_y(x, y, t) = \sum_{m=1}^{\infty} \sum_{n=1}^{\infty} y_{mn} \sin \alpha x \cos \beta y e^{i\omega t}. \quad (67)$$

The force can also be calculated from the following relations:

$$q = \sum_{m=1}^{\infty} \sum_{n=1}^{\infty} Q_{mn} \sin \alpha x \sin \beta y, \quad (68)$$

$$Q_{mn} = \frac{4}{ab} \int_0^a \int_0^b q(x, y) \sin \alpha x \sin \beta y dx dy, \quad (69)$$

$$Q_{mn} = \begin{cases} q_0; & \text{For sinusoidal force} \\ \frac{16q_0}{mn\pi^2}; & \text{For uniform force} \\ \frac{4Q_0}{ab} \sin \frac{m\pi}{2} \sin \frac{n\pi}{2}; & \\ \text{For point force in the plane center} \end{cases}, \quad (70)$$

where:

$$\alpha = \frac{\pi m}{a}, \beta = \frac{\pi n}{b}, i = \sqrt{-1}. \quad (71)$$

Simply-supported boundary conditions were also satisfied by the Navier's method according to the following equations:

$$x=0, x=a \begin{cases} w(0, y) = w(a, y) = \\ = \sum \sum w_{mn} \sin \frac{m\pi}{a} x \sin \frac{n\pi}{b} y = 0 \\ \varphi_y(0, y) = \varphi_y(a, y) = \\ = \sum \sum y_{mn} \sin \frac{m\pi}{a} x \cos \frac{n\pi}{b} y = 0 \end{cases}, \quad (72)$$

$$y = 0, y = b \left\{ \begin{aligned} w(x, 0) = w(x, b) = \\ = \sum \sum w_{mn} \sin \frac{m\pi}{a} x \sin \frac{n\pi}{b} y = 0 \\ \varphi_x(x, 0) = \varphi_x(x, b) = \\ = \sum \sum X_{mn} \cos \frac{m\pi}{a} x \sin \frac{n\pi}{b} y = 0 \end{aligned} \right. , \quad (73)$$

**9. The general equation matrix of a Mindlin's plane**

After solving the governing equations and naming the coefficient of each variable, we have:

$$U = 2C\alpha\beta + C\alpha + C\beta + C\alpha + C\beta , \quad (74)$$

$$U = U = -C\alpha - C\alpha\beta + C\alpha , \quad (75)$$

$$U_3 = U_7 = -C_1\beta^3 - C_1\alpha^2\beta + C_2\beta , \quad (76)$$

$$U_5 = -C_3\beta^4 - C_3\alpha^2\beta^2 - C_4\beta^2 - C_5\alpha^2 + C_2 , \quad (77)$$

$$U_6 = C_3\alpha\beta^3 + C_3\alpha^3\beta - C_6\alpha\beta , \quad (78)$$

$$U_8 = -C_3\alpha^3\beta - C_3\alpha\beta^3 - C_6\alpha\beta , \quad (79)$$

$$U_9 = C_3\alpha^4 + C_3\alpha^2\beta^2 - C_4\alpha^2 - C_5\beta^2 + C_2 , \quad (80)$$

$$K_1 = -C_7 \quad (81)$$

$$K_2 = K_3 = K_4 = K_6 = K_7 = K_8 = 0 , \quad (82)$$

$$K_5 = K_9 = -C_8 . \quad (83)$$

Finally, the general equation matrix of the Mindlin's plate along with the auxiliary equations will be obtained as follows:

$$\left( \begin{bmatrix} U_1 & U_2 & U_3 \\ U_4 & U_5 & U_6 \\ U_7 & U_8 & U_9 \end{bmatrix} - \omega^2 \begin{bmatrix} K_1 & K_2 & K_3 \\ K_4 & K_5 & K_6 \\ K_7 & K_8 & K_9 \end{bmatrix} \right) \begin{bmatrix} w_{mn} \\ X_{mn} \\ y_{mn} \end{bmatrix} = \begin{bmatrix} Q_{mn} \\ 0 \\ 0 \end{bmatrix} . \quad (84)$$

In this study, graphene is chosen as the plate's material. A single-layer graphene plate has the following properties [9]:  $E=1.06$  TPa,  $\nu = 0.25$ ,  $h=0.34$  nm,  $r=2250$  kg/m.

Also, the relationship between  $E$ ,  $\mu$  and  $\nu$  can be expressed as:

$$\lambda = \frac{\nu E}{(1+\nu)(1-2\nu)} , \mu = \frac{E}{2(1+\nu)} , \quad (85)$$

where:  $\mu$  and  $\lambda$  are the lame's coefficients;  $E$  is the Young's modulus [10]. The value of the distributed force was considered to be  $q = 1$  N/m .

**10. Results and discussion**

Results were obtained using a computational program coded in the MATLAB software. The results have also been compared with the literature [11, 12] and good agree-

ments between results were observed. The plate's dimensional parameters are chosen as follows:  $a$  is plate's length;  $b$  is plate's width;  $h$  is plate's thickness;  $l$  is material length scale parameter

Table 1 shows the Mindlin's nanoplate bending rate under sinusoidal load for different material length scale parameters to thickness  $l/h$  and length to width ratio  $a/b$ . As can be seen, as the length scale parameter to thickness ratio increases, the bending ratio decreases but it increases due to the increase in the plate's length to width ratio.

Table 1

The Mindlin's nanoplate bending rate under sinusoidal load for different length to width and material length scale to thickness ratios ( $q = 1e - 18$  N/nm ,  $a / h = 30$ )

a/b	l/h			
	0	0.5	1	2
1	7.0630	1.6642	0.5104	0.1406
1.5	14.2905	3.3664	1.0306	0.2820
2	21.1039	4.9708	1.5205	0.4145

Table 2 compares the values of critical force for different nanoplates under a bi-axial surface loading for various length to thickness ratios. It was observed that, the Mindlin's nanoplate has the highest, and the Third-order nanoplate has the lowest critical force values.

Table 2

Values of the critical force for different nanoplates under a bi-axial surface loading for various width to thickness ratios ( $P_y/P_x=1, l/h=1, a/b=1$ )

a/h	Kirchhoff plate	Mindlin plate	Third order shear deformation plate	N order shear deformation plate (n=5)
5	142.2802	233.7327	130.1058	131.5295
10	35.5701	86.0362	34.7400	34.8479
20	8.8925	23.9784	8.8394	8.8465
30	3.9522	10.8814	3.9417	3.9431
40	2.2231	6.16595	2.2198	2.2202
50	1.4228	3.9597	1.4214	1.4216

Fig. 2 compares the bending values of different nanoplates under the uniform surface traction for different length to width ratios. As can be seen, the Kirchhoff's nanoplate yielded the lowest values and the third-order nanoplate yielded the highest values for bending.

Table 3 shows the dimensionless bending values of Mindlin's nanoplate under the uniform surface traction and sinusoidal load for material length scale to thickness and length to width ratios. As shown in the table, except for the classical theory  $l=0$ , the dimensionless bending values under sinusoidal load were higher than bending values obtained under the uniform surface traction. It was also found that with an increase in the material length scale parameter to thickness and length to width ratio of the nanoplate, the dimensionless bending value decreases.

Fig. 3 shows the values of dimensionless critical force for Mindlin's nanoplate under a uniaxial force in the x-direction. It was found that this value increases due to an increase in length to thickness ratio of the nanoplate. Furthermore, when the effect of size parameter is neglected (classical theory), the value of dimensionless critical force becomes constant and reaches its lowest value, but with an increase in the size parameter the dimensionless critical force value increases.

The dimensionless bending values of Mindlin's nanoplate under uniform surface traction and sinusoidal load for various material length scale to thickness and length to width ratios ( $a/h = 30, q = 1e-18N/nm$ )

a/b	l/h							
	0		0.5		1		2	
	Uniform load	Sinusoidal load						
1	1	1	0.235573	0.235626	0.072128	0.072264	0.019740	0.019913
1.5	1	1	0.235499	0.235569	0.071942	0.072121	0.019506	0.019735
2	1	1	0.235479	0.235541	0.071892	0.072049	0.019443	0.019643

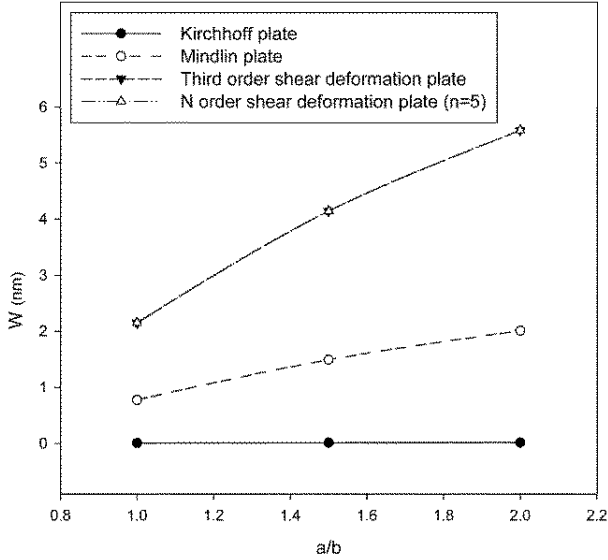


Fig. 2 Comparison of bending values for different nanoplates under the uniform surface traction for different aspect ratios ( $a/h = 30, l/h = 1, q = 1e-18N/nm$ )

thickness of the nanoplate.

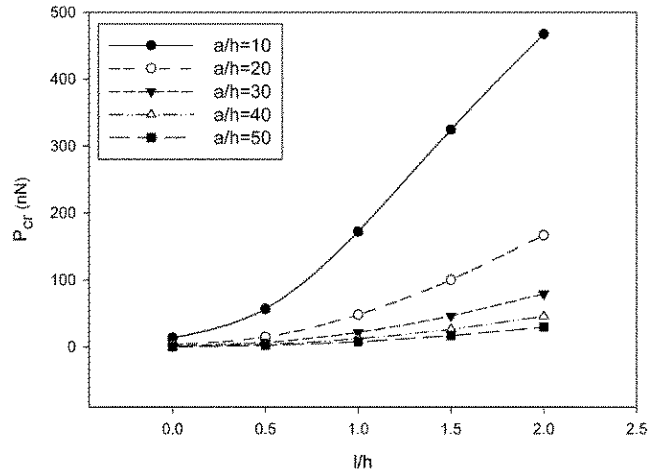


Fig. 4 Values of critical force for Mindlin's nanoplate under a uniaxial force in the  $x$ -direction for various material length scale to thickness and length to thickness ratio of the nanoplate ( $a/b=1, m=1, n=1$ )

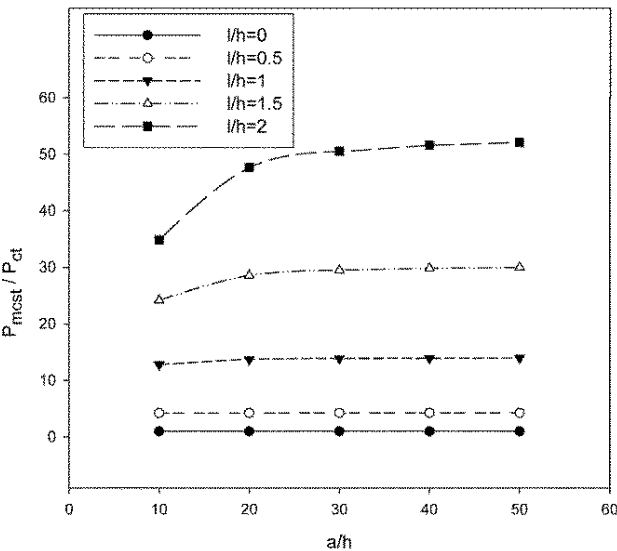


Fig. 3 Values of dimensionless critical force for Mindlin's nanoplate under a uniaxial force in the  $x$ -direction for different material length scale to thickness and length to thickness ratio of the nanoplate ( $a/b=1, m=1, n=1$ )

Fig. 4 shows the values of critical force for Mindlin's nanoplate under a uniaxial force in the  $x$ -direction. As shown in the figure, the dimensionless critical force increases due to an increase in the length scale parameter to thickness ratio and decreases due to an increase in length to

Fig. 5 shows the values of dimensionless critical force for Mindlin's nanoplate under a bi-axial surface force in  $x$  and  $y$  directions. As can be seen, this value increases due to an increase in, length scale parameter to thickness and length to thickness ratio of nanoplate.

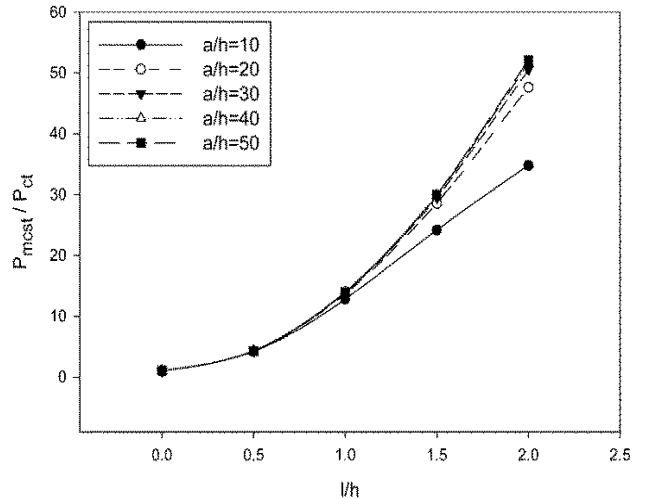


Fig. 5 Values of dimensionless critical force for Mindlin's nanoplate under a bi-axial surface force in  $x$  and  $y$  directions for material length scale to thickness and length to thickness ratio of the nanoplate ( $a/b=1, m=1, n=1$ )

Figs. 6 – 9 shows the dimensionless frequency of

different modes of Mindlin's nanoplate ( $\omega_{11} / \omega_c - \omega_{12} / \omega_c - \omega_{21} / \omega_c - \omega_{22} / \omega_c$ ) (except for the classical theory  $l=0$ ). It was observed that this value increases due to an increase in length to thickness ratio. Also, for the classical theory (neglecting the effect of size parameter) the dimensionless frequency reaches its lowest value, but with an increase in the size effect, the dimensionless frequency values increase.

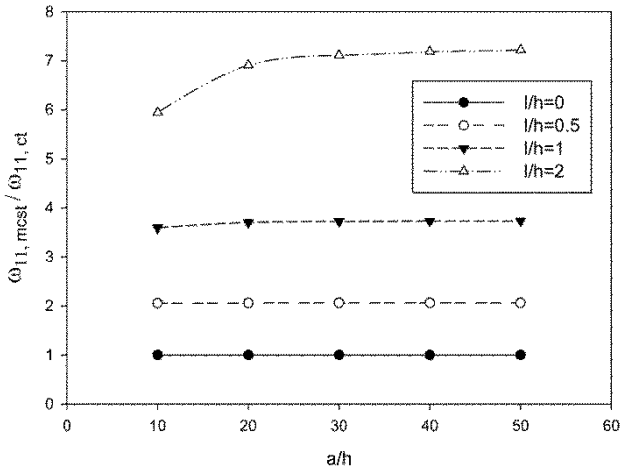


Fig. 6 Comparison of dimensionless frequencies of the first mode ( $\omega_{11}$ ) for a Mindlin's nanoplate for various material length scale parameter to thickness and length to thickness ratios of the nanoplate ( $h=0.34, a/b=1$ )

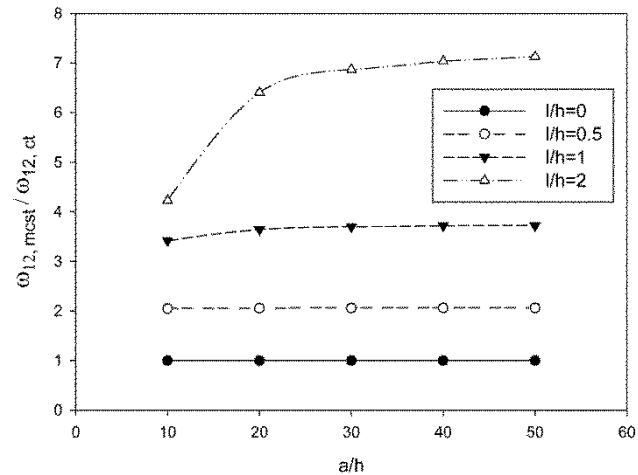


Fig. 7 Comparison of dimensionless frequencies of the mode ( $\omega_{12}$ ) for a Mindlin's nanoplate various material length scale parameter to thickness and length to thickness ratios of the nanoplate ( $h=0.34, a/b=1$ )

Table 4 shows that the dimensionless frequency of different modes of Mindlin's nanoplate increases due to an increase in material length scale parameter to thickness ratio.

By comparing Tables 4 – 7 it was found that with an increase in length to thickness ratio of the Mindlin's nanoplate, the vibration frequency decreases.

Table 8 shows different modes of frequencies for various nanoplates ( $\omega_{11} - \omega_{12} - \omega_{21} - \omega_{22}$ ). According to the table, the frequency values were the highest for the Mindlin's nanoplate and the lowest for the third-order nanoplate.

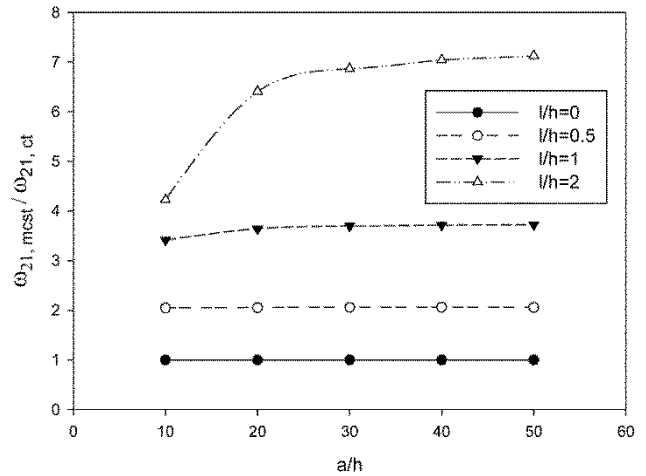


Fig. 8 Comparison of dimensionless frequencies of the mode ( $\omega_{21}$ ) for a Mindlin's nanoplate for various material length scale parameter to thickness and length to thickness ratios of the nanoplate ( $h=0.34, a/b=1$ )

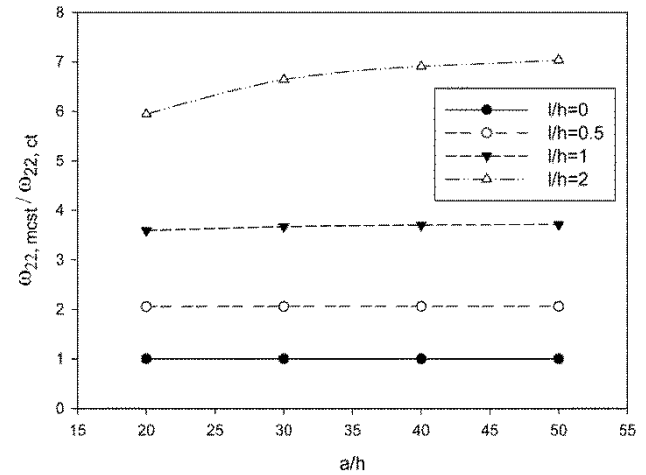


Fig. 9 Comparison of dimensionless frequencies of the mode ( $\omega_{22}$ ) of a Mindlin's nanoplate for various material length scale parameter to thickness and length to thickness ratios of the nanoplate ( $a/h=0.34, a/b=1$ )

Table 4

Comparison of dimensionless frequencies of different modes of Mindlin's nanoplate for various material length to thickness ratios ( $a/b=1, a/h=30$ )

Mode	l/h			
	0	0.5	1	2
$\omega_{11}$	13.9429	28.7266	51.9052	99.1252
$\omega_{12}$	34.6425	71.3140	128.0217	237.9174
$\omega_{21}$	34.6425	71.3140	128.0217	237.9174
$\omega_{22}$	55.0918	113.3246	202.1703	365.8010
$\omega_{33}$	121.5505	249.5297	436.5378	722.2380

Table 5

Comparison of dimensionless frequencies of different modes of Mindlin's nanoplate for various material length to thickness ratios ( $a/b=1.5, a/h=30$ )

Mode	l/h			
	0	0.5	1	2
$\omega_{11}$	10.0816	20.7745	37.5829	72.1427
$\omega_{12}$	19.3340	39.8248	71.8354	136.2116

Continuation of Table 5

Mode	$l/h$			
	0	0.5	1	2
$\omega_{21}$	30.8284	63.4718	114.0783	213.0666
$\omega_{22}$	39.9678	82.2599	147.4292	272.0827
$\omega_{33}$	88.6398	182.1338	321.6951	556.8022

Table 6

Comparison of dimensionless frequencies of different modes of Mindlin's nanoplate for various length to thickness ratios ( $a/b=0.5$ ,  $l/h=1$ )

Mode	$a/h$			
	20	30	40	50
$\omega_{21}$	280.4153	128.0217	72.7219	46.7575
$\omega_{12}$	436.5378	202.1703	115.4757	74.4444
$\omega_{21}$	860.2980	413.9252	240.0504	155.9272
$\omega_{22}$	988.5087	481.2484	280.4153	182.5827
$\omega_{33}$	1844.9056	988.5087	596.8069	395.7091

Table 7

Comparison of dimensionless frequencies of different modes of Mindlin's nanoplate for length to thickness ratio ( $a/b=1$ ,  $l/h=1$ )

Mode	$a/h$			
	20	30	40	50
$\omega_{11}$	115.4757	51.9052	29.3145	18.7965
$\omega_{12}$	280.4153	128.0217	72.7219	46.7575
$\omega_{21}$	280.4153	128.0217	72.7219	46.7575
$\omega_{22}$	436.5378	202.1703	115.4757	74.4444
$\omega_{33}$	903.7094	436.5378	253.5674	164.8397

Table 8

Comparison of dimensionless frequencies of different modes of various nanoplates for length to thickness ratio ( $a/b=1$ ,  $l/h=1$ )

Mode	$l/h$		
	20	30	40
Mindlin plate			
$\omega_{11}$	280.4153	128.0217	72.7219
$\omega_{12}$	436.5378	202.1703	115.4757
$\omega_{21}$	860.2980	413.9252	240.0504
$\omega_{22}$	988.5087	481.2484	280.4153
Kirchhoff plate			
$\omega_{11}$	175.2090	78.0917	43.9704
$\omega_{12}$	279.4825	124.7767	70.2985
$\omega_{21}$	588.5668	264.0744	149.0415
$\omega_{22}$	690.3772	310.2573	175.2090
Third order shear deformation plate			
$\omega_{11}$	174.0385	77.8533	43.8941
$\omega_{12}$	276.5826	124.1752	70.1049
$\omega_{21}$	576.6542	261.4753	148.1887
$\omega_{22}$	674.3836	306.7113	174.0385

## 11. Conclusion

In this study, the bending, buckling and vibration of a graphene Mindlin's nanoplate were investigated using the modified couple stress theory. As observed in the tables and figures, the Mindlin's nanoplate bending rate under sinusoidal load, decreases with an increase in length to thickness ratio of the nanoplate, but, this value increases with an increase in the aspect ratio of the nanoplate. Furthermore, by comparing different nanoplates under uniform surface traction it was found that the Kirchhoff's nanoplate yields

the lowest and the third-order nanoplate yields the highest values for bending.

The buckling analysis showed that the dimensionless critical force increases due to an increase in material length scale parameter to thickness ratio and decreases due to an increase in length to thickness ratio of the nanoplate. But when the size effect parameter is neglected (classical theory), the value of dimensionless critical force becomes constant and reaches its lowest value, but with an increase in the size parameter the dimensionless critical force value increases.

Analysis of frequencies of different modes showed that this value increases due to an increase in length to thickness ratio. Also, for the classical theory (neglecting the effect of size parameter) the dimensionless frequency reaches its lowest value, but with an increase in the size effect, the dimensionless frequency values increase. It was also found that the Mindlin's nanoplate yields the highest and the third-order nanoplate yields the lowest values for frequency.

## References

1. **Yang, F. A. C. M.; Chong, A. C. M.; Lam, D. C. C.; Tong, P.** 2002. Couple stress based strain gradient theory for elasticity, *International Journal of Solids and Structures* 39(10): 2731-2743. [https://doi.org/10.1016/S0020-7683\(02\)00152-X](https://doi.org/10.1016/S0020-7683(02)00152-X).
2. **Toupin, R.A.** 1962. Elastic materials with couple stresses, *Arch. Rational Mech. Anal.* 11: 385-414.
3. **Mindlin, R. D.; Tiersten, H. F.** 1962. Effects of couple-stresses in linear elasticity, *Columbia Univ., New York CU-TR-48*.
4. **Koiter, W. T.** 1969. Couple-stresses in the theory of elasticity, I & II. *Proc. K. Ned. Akad. Wet. (B)* 67: 17-44.
5. **Mindlin, R. D.** 1963. Microstructure in linear elasticity, *C. Columbia Univ., New York Dept. of Civil Engineering and Engineering Mechanics TR-50*.
6. **Tsiatas, G. C.** 2009. A new Kirchhoff plate model based on a modified couple stress theory, *International Journal of Solids and Structures* 46(13): 2757-2764. <https://doi.org/10.1016/j.ijsolstr.2009.03.004>.
7. **Wang, B.; Zhou, S.; Zhao, J.; Chen, X.** 2011. A size-dependent Kirchhoff micro-plate model based on strain gradient elasticity theory, *European Journal of Mechanics-A/Solids* 30(4): 517-524. <https://doi.org/10.1016/j.euromechsol.2011.04.001>.
8. **Thai, H. T.; Choi, D. H.** 2013. Size-dependent functionally graded Kirchhoff and Mindlin plate models based on a modified couple stress theory, *Composite Structures* 95: 142-153. <https://doi.org/10.1016/j.compstruct.2012.08.023>.
9. **Akgöz, B.; Civalek, Ö.** 2012. Free vibration analysis for single-layered graphene sheets in an elastic matrix via modified couple stress theory, *Materials & Design* 42: 164-171. <https://doi.org/10.1016/j.matdes.2012.06.002>.
10. **Roque, C. M. C.; Ferreira, A. J. M.; Reddy, J. N.** 2013. Analysis of Mindlin micro plates with a modified couple stress theory and a meshless method, *Applied Mathematical Modelling* 37(7): 4626-4633. <https://doi.org/10.1016/j.apm.2012.09.063>.
11. **Zhang, B.; He, Y.; Liu, D.; Shen, L.; Lei, J.** 2015. An efficient size-dependent plate theory for bending, buck-

- ling and free vibration analyses of functionally graded microplates resting on elastic foundation, *Applied Mathematical Modelling* 39: 3814-3845.  
<https://doi.org/10.1016/j.apm.2014.12.001>.
12. **Jung, W. Y; Han, S. C; Park, W. T.** 2014. A modified couple stress theory for buckling analysis of S-FGM nanoplates embedded in Pasternak elastic medium, *Composites Part B: Engineering* 60: 746-756.  
<https://doi.org/10.1016/j.compositesb.2013.12.058>.

M. Eskandari Shahraki, M. Shariati, N. Asiaban, J. Eskandari Jam

BENDING, BUCKLING AND VIBRATIONS ANALYSIS OF THE GRAPHENE NANOPATE USING THE MODIFIED COUPLE STRESS THEORY

S u m m a r y

In this paper a Mindlin's plate model is developed for the Bending, buckling and vibration analysis of a graphene nanoplate based on a modified couple stress theory. The bending rates and dimensionless bending values under uniform surface traction and sinusoidal load, the dimensionless critical force under a bi-axial surface force in  $x$  and  $y$  directions and dimensionless frequencies of different modes are all obtained for various plate's dimensional ratios and material length scale to thickness ratios. The results are presented and discussed in details.

**Keywords:** modified couple stress theory, mindlin plate, rectangular nanoplate, Navier type solution.

Received August 23, 2020

Accepted October 04, 2021



This article is an Open Access article distributed under the terms and conditions of the Creative Commons Attribution 4.0 (CC BY 4.0) License (<http://creativecommons.org/licenses/by/4.0/>).